frontiers | Frontiers in Earth Science

ORIGINAL RESEARCH
published: 16 June 2022
doi: 10.3389/feart.2022.914426

Sedimentology and Geochemistry of the Upper Permian Linghao Formation Marine Shale, Central Nanpanjiang Basin, SW China

Yifan Gu[1,2], *Dongfeng Hu*[3], *Zhihong Wei*[3], *Ruobing Liu*[3], *Jingyu Hao*[3], *Jing Han*[3], *Zhiwei Fan*[3], *Yuqiang Jiang*[1,2]*, *Yansong Wang*[1,2] *and Qidi Xu*[1,2]

[1]School of Geoscience and Technology, Southwest Petroleum University, Chengdu, China, [2]The Unconventional Reservoir Evaluation Department, PetroChina Key Laboratory of Unconventional Oil and Gas Resources, Chengdu, China, [3]Exploration Company, Sinopec, Chengdu, China

The Upper Permian Linghao Formation marine shale and contemporaneous transitional shale are the most potential shale gas targets in the Nanpanjiang basin, which is characterized by considerable TOC content, wide distribution, and considerable shale thickness. On the basis of division in Linghao Formation, petrographic, mineralogical, and high-resolution geochemical analyses were integrated to reveal the sedimentary environment including paleoproductivity, paleoredox conditions, detrital influx, paleoclimate, and the paleosalinity. There are two organic-rich shale intervals in Linghao Formation, which are Ling 1 member and the lower Ling 3 member. The lower Ling 1 is dominated by deep-water shelf facies, which are characterized by high TOC value (0.93%–6.36%, avg. 2.43%), high detrital influx proxies (Zr, 746–1508 ppm, avg. 1093 ppm; Ti, 19278–128730 ppm, avg. 16091 ppm), relatively warm–humid paleoclimate condition (CIA*, 75.94-91.90, avg. 82.26), low paleosalinity proxies (Sr/Ba, 0.13-0.34, avg. 0.22), and high paleoproductivity (P/Al (10^{-2}), 1.06-2.06, avg. 1.63; Mn/Ca (10^{-3}), 27.37-291.69, avg. 128.07). Detrital influx including gravity flow plays a critical role in the enrichment of organic matter. The sedimentary environment of upper Ling 1 and lower Ling 3 is the same as that of lower Ling 1. Unlike lower Ling 1, these intervals are characterized by low detrital influx proxies, moderate weathering, and relatively high paleosalinity proxies. The volcanic ash of Emei volcanism and felsic volcanism in South China plays a critical role in the enrichment of organic matter in upper Ling 1 and lower Ling 3, respectively. The sedimentary models for Linghao Formation organic-rich shale can reveal factors controlling the enrichment of organic matter.

Keywords: upper permian, sedimentology, geochemistry, marine shale, Linghao formation, Nanpanjiang basin

OPEN ACCESS

Edited by:
Shu Jiang,
The University of Utah, United States

Reviewed by:
Qingshao Liang,
Chengdu University of Technology, China
Zhaodong Xi,
China University of Geosciences, China
Lei Chen,
China University of Petroleum, Huadong, China

***Correspondence:**
Yuqiang Jiang
xnsyjyq3055@126.com

Specialty section:
This article was submitted to Economic Geology, a section of the journal Frontiers in Earth Science

Received: *06 April 2022*
Accepted: *05 May 2022*
Published: *16 June 2022*

Citation:
Gu Y, Hu D, Wei Z, Liu R, Hao J, Han J, Fan Z, Jiang Y, Wang Y and Xu Q (2022) Sedimentology and Geochemistry of the Upper Permian Linghao Formation Marine Shale, Central Nanpanjiang Basin, SW China. Front. Earth Sci. 10:914426. doi: 10.3389/feart.2022.914426

INTRODUCTION

Shale oil and gas resources have been a significant part of unconventional resources in recent years (Jia, 2017; Liang et al., 2018). Organic-rich marine shales are the main target rocks for the exploration and development of unconventional hydrocarbon resources (Clarkson et al., 2012; Zou et al., 2019; Qiu and Zou, 2020; Xi et al., 2022; Zhang et al., 2022). In China, a total of 12 important organic-rich marine shale units are recognized in Mesoproterozoic through Cenozoic strata (Zou et al., 2019).

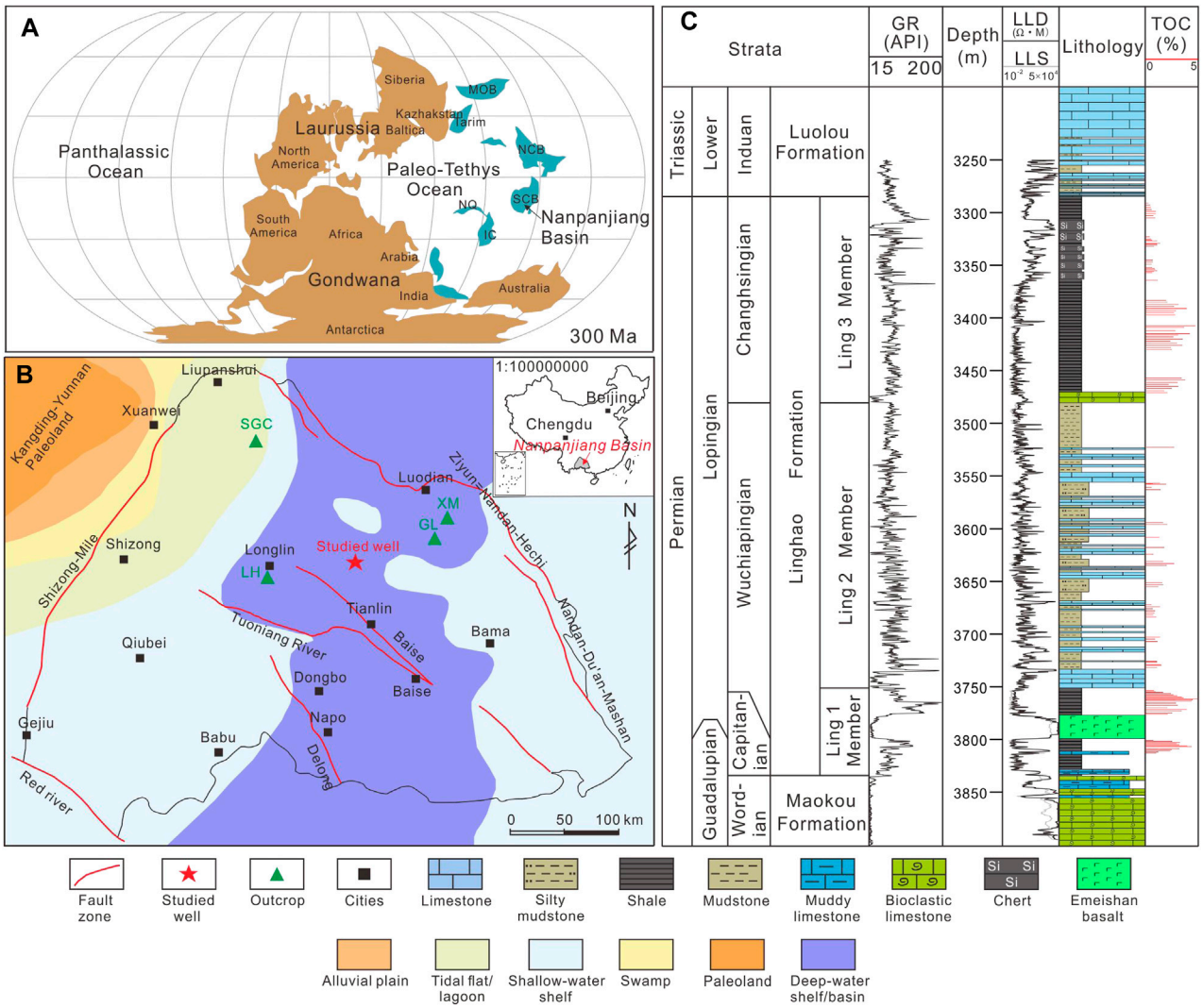

FIGURE 1 | (A) Paleogeographic reconstructions of the Eastern Asian blocks at 300 Ma with respect to the Nanpanjiang basin. IC, MOB, NCB, NQ, Qm, and SCB represent the Indochina, Mongolian, North China, North Qiangtang, Qaidam, and South China blocks/terranes (modified from Huang et al., 2018). **(B)** Location of the Nanpanjiang basin, Southwest China (modified from Xia et al., 2018). **(C)** Generalized stratigraphy of Upper Permian Linghao Formation in the study area (based on the studied well).

Under the exemplary role of the United States' "shale gas revolution" (Chen et al., 2019a; Chen et al., 2019b; Chen et al., 2019c), China has achieved a breakthrough in shale gas industrialization since 2010 (Jia, 2017; Xi et al., 2017; Xi et al., 2018). Weiyuan, Changning, Jiaoshiba, and other shale gas fields have been built, and large-scale shale gas development has been realized in marine organic-rich shales of the Late Ordovician–early Silurian (Zhang et al., 2019a; Zhang et al., 2019b; Zou et al., 2019; Zhang et al., 2020a; Chen et al., 2021). The studies on this set of shale are abundant and various, which lays a good foundation for efficient exploration and development (Zhang et al., 2020b; Zhang et al., 2020c). Permian marine or transitional organic-rich shale in South China is characterized by extensive distribution, considerable TOC content, and shale thickness, which is the most promising alternative strata for future shale gas exploration in China (Liu et al., 2013; Han et al., 2017). However, this set of shale is still in the early stage of exploration, and the lack of relevant studies seriously restricts the progress of shale gas exploration. Scientific problems such as spatial distribution, microscopic pore structure, and genesis of Permian organic-rich shale need to be solved first.

Geochemical proxies have been widely used to illustrate the effect of paleoproductivity, paleoredox condition, paleosalinity, and terrigenous input on the deposition of organic-rich shales (Ding et al., 2018; He et al., 2020; Liang et al., 2020; Leifu Zhang et al., 2021). Based on the division of the Linghao Formation in central Nanpanjiang basin, macroscopic sedimentary characteristics, microscopic petrological characteristics, and high-resolution geochemical analyses are integrated into this study to reveal depositional conditions (including terrigenous

input, paleoclimate condition, paleosalinity, paleoproductivity, and paleoredox) of different members in Linghao Formation. This study aims to reveal the distribution and genesis of marine-hosted organic-rich shale in the Permian Linghao Formation and provide scientific guidance for shale gas exploration of Permian marine.

GEOLOGICAL BACKGROUND

The Nanpanjiang basin, with an area of 380, 000 km^2, is located at the junction of Yunnan, Guizhou, and Guangxi, and the geotectonic position is located on the southwestern margin of South China Block (Xia et al., 2018) (**Figures 1A,B**). Similar to the Carboniferous Datang Formation in the Nanpanjiang basin, the Linghao Formation is a special and representative stratigraphic unit formed by the deep-water sedimentary environment between isolated platforms during the late Permian. Observations from the studied well and outcrops show that the Linghao Formation is in conformable contact with underlying limestone or muddy limestone of the Maokou Formation, and the overlying Luolou Formation. According to the combination of lithology, logging characteristics, and lithology, the Linghao Formation can be divided into Ling 1 member, Ling 2 member, and Ling 3 member. The Ling 1 member consists of shale with Emeishan basalt interbed. Previous studies suggested that the eruption timing of Emeishan basalt is between 257 Ma and 259 Ma (Shellnutt et al., 2012), and its formation period belongs to Wuchiapingian. The Ling 2 member is composed of mudstone and limestone. The Ling 3 Member is composed of shale (**Figure 1C**). According to previous studies, the northwest Nanpanjiang basin is dominated by swamp, tidal flat, and lagoon facies during Linghao period (Luo et al., 2018; He et al., 2020). The contemporaneous strata of the Linghao period comprise mudstones, silty mudstones, siltstones, limestones, and coals (He et al., 2020). The studied well is located in the central Nanpanjiang basin which is dominated by shelf facies during Linghao deposition (**Figure 1B**).

SAMPLES AND METHODS

Sedimentological Characterization

The study was well carried out continuous coring in Linghao Formation. Macroscopic observation of core and outcrops identified different rock types, including limestone, mudstone, silty mudstone, and shale, and record the lithology combination of different members. 150 core samples were made into thin sections and the core observation results were further verified by a Leica DM4 M optical microscope. Macroscopic characteristics of sedimentary texture or structure in typical outcrops were described in the study, with emphasis on the difference between each member of the Linghao Formation.

Organic Matter Content Analysis

TOC was measured by a Leco carbon/sulfur analyzer in the State Key Laboratory of Oil and Gas Reservoir Geology and Exploitation of China, and the analytical precisions are ±0.5%. 116 samples were treated with 10% hydrochloric acid to remove carbonates. The acid-treated sample was washed with distilled water to neutral, then the sample was dried in an oven at 60°C–80°C. Dried samples were added to the cosolvent and fully burned in the high-temperature oxygen flow, ensuring that the organic carbon can be completely converted into carbon dioxide, and the content of total organic carbon was tested by the infrared detector.

Major Element Composition Analysis

The content of major elements (Al, Si, Ti, Ca, Fe, Mg, Mn, K, and Na) was determined by X-ray fluorescence (XRF) spectroscopy. 60 powder samples were used to eliminate the mineral and particle size effects and cast to suitable fused glass beads to fit the X-ray fluorescence spectrometer. The fluorescent X-ray intensity of the elements was measured. Based on the calibration curve or equation, the interference effect between elements was corrected and the element content was obtained. The accuracy of the XRF analysis is better than 1% for all major oxides.

Paleoclimate conditions were evaluated by the chemical index of alteration (CIA), which was calculated using the following formula (Nesbitt and Young, 1982; Price and Velbel, 2003; Liu et al., 2017):

$$CIA^{*} = 100 \times Al_2O_3 / (Al_2O_3 + Na_2O + K_2O). \quad (1)$$

Trace Element Composition Analysis

Trace elemental contents were measured by using inductively coupled plasma-mass spectrometry (ICP-MS). 60 samples were dissolved with hydrofluoric acid and nitric acid in a closed container. The hydrofluoric acid was wiped out by evaporation on the electric heating plate and then dissolved by nitric acid. After dilution, the samples were directly measured by ICP-MS. The analytical uncertainties are estimated to be 5%. Standard rock reference material (GSD-9) was used to monitor the analytical accuracy and precision.

Authigenic enrichment of redox-sensitive trace elements was widely used to indicate redox changes in the water column (Algeo and Tribovillard, 2009; Algeo and Liu, 2020). The enrichment factor (EF) is calculated by comparing the Al-normalized metal content to that of the continental crust (Wedepohl, 1995). The calculation formula is as follows:

$$X_{EF} = (X/A1)_{sample} / (X/A1)_{CC}. \quad (2)$$

In the formula, X represents the content of element X, and $(X/Al)_{CC}$ represents the X/Al ratio of the continental crust (Wedepohl, 1995).

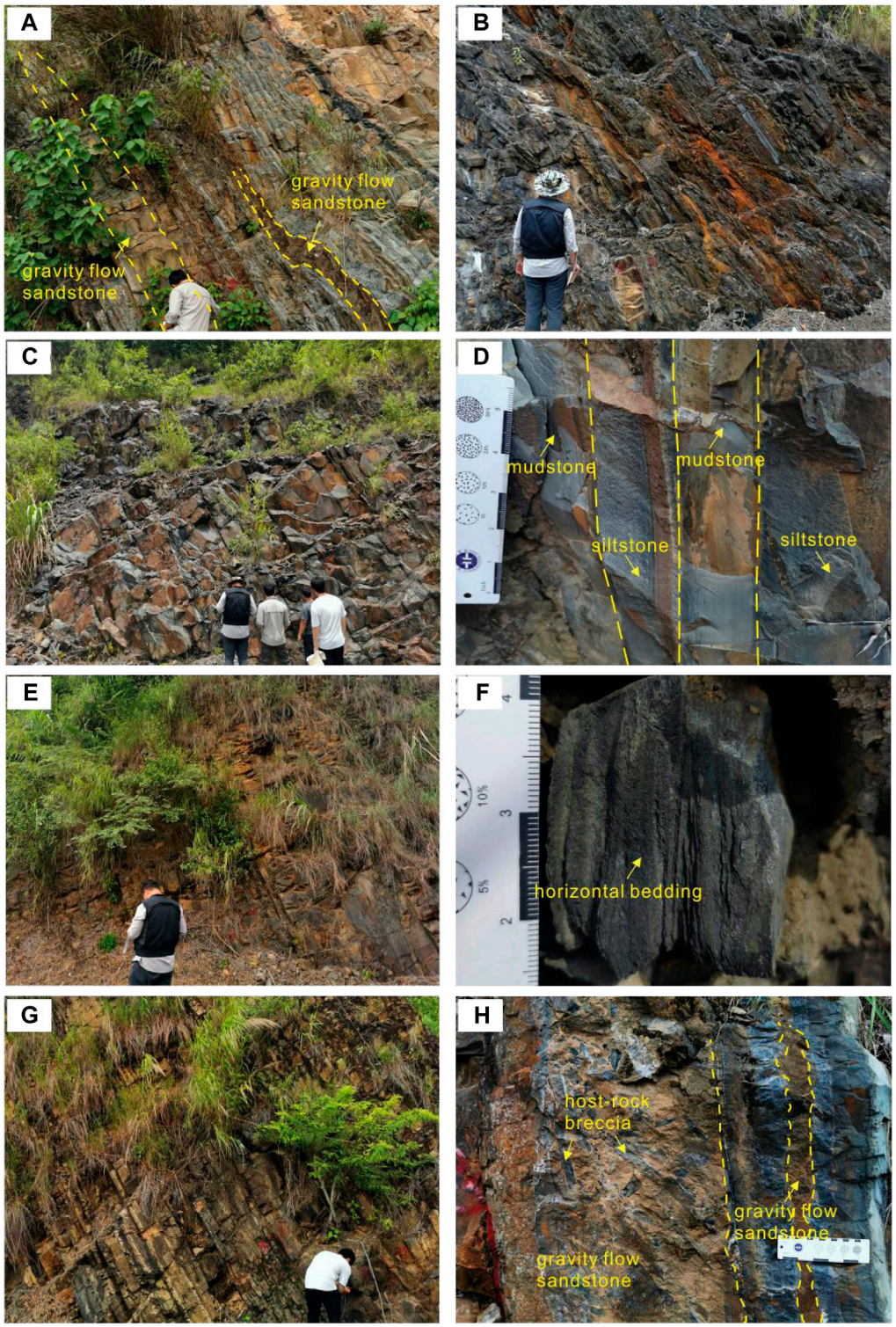

FIGURE 2 | Macroscopic sedimentary characteristics for Linghao Formation from typical outcrops in the central Nanpanjiang basin. **(A)** Gravity flow sandstone in black shale, lower Ling 1 member, XM Outcrop. **(B)** Black shale with abundant organic matter in upper Ling 1 member, XM Outcrop. **(C)** Grey mudstone and silty mudstone with interbed of siltstone, Ling 2 member, XM Outcrop. **(D)** Frequent thin interbeds between siltstone and mudstone, Ling 2 member, GL Outcrop. **(E)** Black shale, lower Ling 3 member, XM Outcrop. **(F)** Black shale with horizontal bedding, lower Ling 3 member, XM Outcrop. **(G)** Chert with horizontal bedding, upper Ling 3 member, XM Outcrop. **(H)** Gravity flow sandstone in chert and host-rock breccia in gravity flow sandstone, upper Ling 3 member, XM Outcrop.

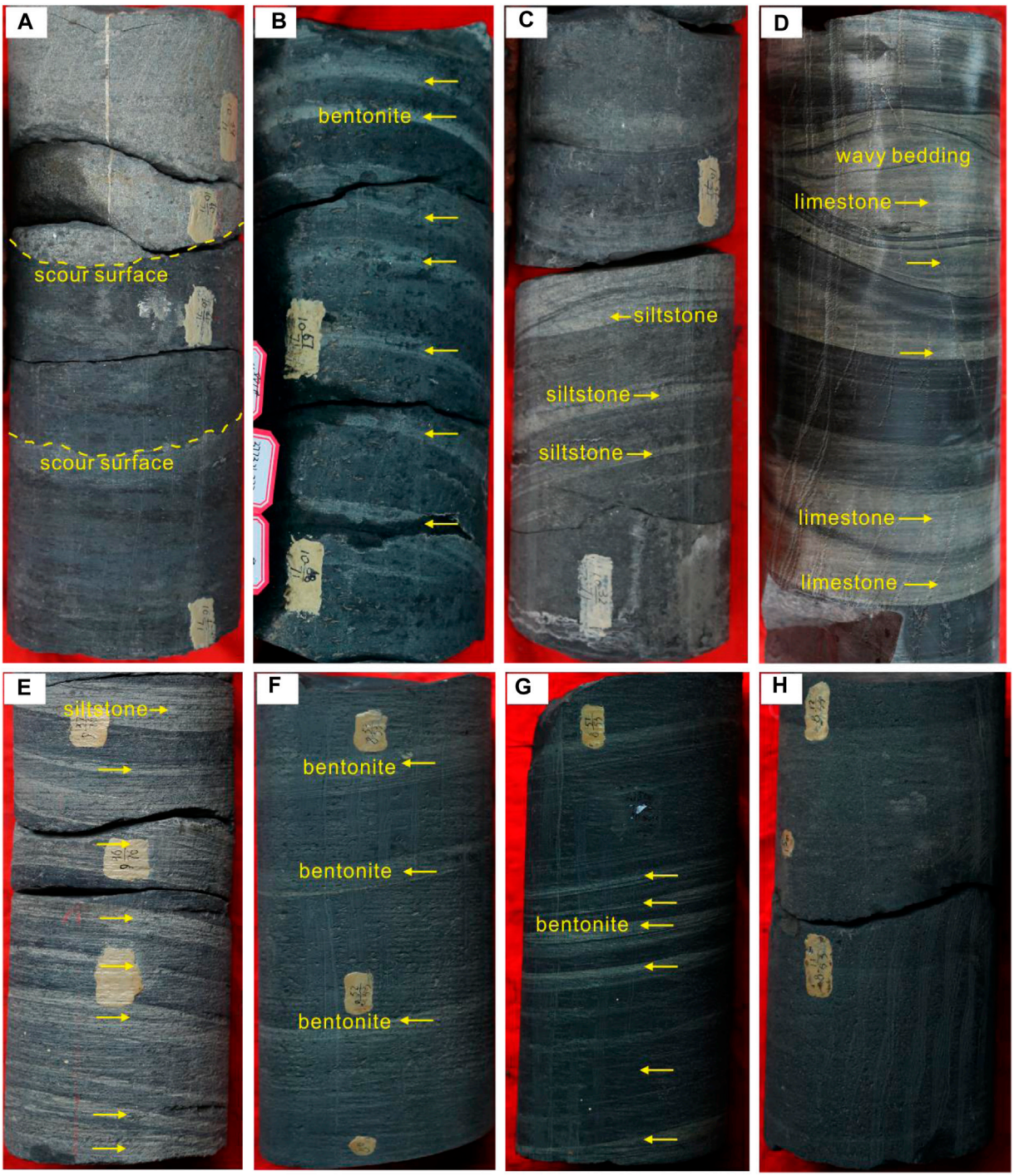

FIGURE 3 | Macroscopic sedimentary characteristics for Linghao Formation from the studied well in the central Nanpanjiang basin. **(A)** Scour surface between black shale and gravity flow sandstone, lower Ling 1 member, 3,803 m–3803.23 m. **(B)** Frequent thin interbeds of bentonite in black shale, upper Ling 1 member, 3,772.88 m–3773.21 m. **(C)** Frequent thin interbeds of siltstone, Ling 2 ember, 3,558.63 m–3559.19 m. **(D)** Frequent thin interbeds of limestone and wavy bedding, Ling 2 Member, 3,738.13 m–3738.42 m. **(E)** Frequent thin interbeds of siltstone in mudstone, Ling 2 Member, 3,559.57 m–3559.92 m. **(F)** Frequent thin interbeds of bentonite, lower Ling 3 Member, 3,414.91 m–3415.22 m. **(G)** Frequent thin interbeds of bentonite, lower Ling 3 Member, 3,414.62 m–3414.91 m. **(H)** Black shale with massive bedding, lower Ling 3 Member, 3,412.12 m–3412.30 m.

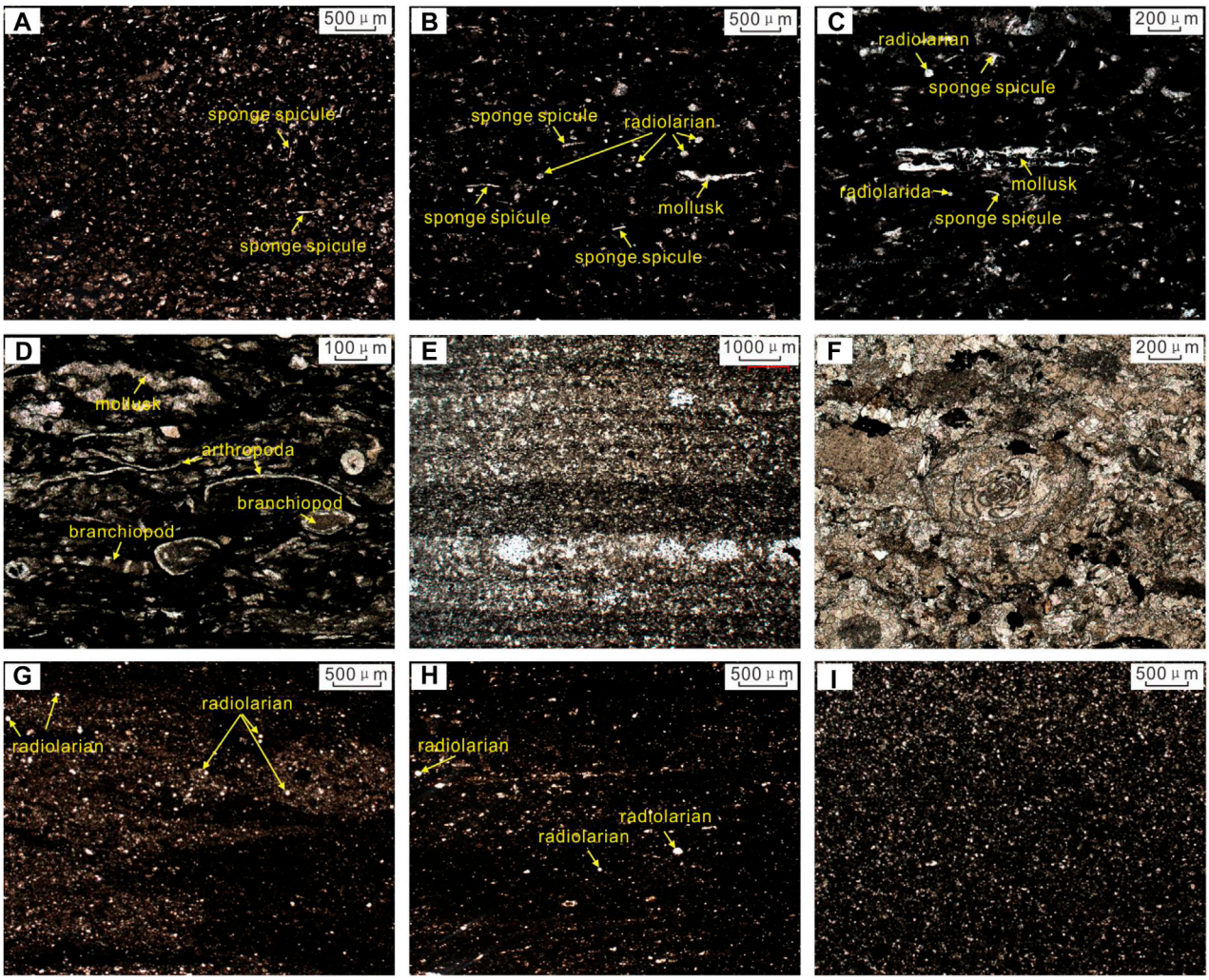

FIGURE 4 | Microscopic characteristics for Linghao Formation from the studied well in the central Nanpanjiang basin. **(A)** Sponge spicule in marine shale, upper Ling 1 Member, 3,772.88 m, plane-polarized light. **(B)** Marine bioclasts including sponge spicule, radiolarian, and mollusk, upper Ling 1 Member, 3773 m, plane-polarized light. **(C)** marine shale containing abundant marine bioclasts including sponge spicule, radiolarian, and mollusk, upper Ling 1 Member, 3,772.97 m, plane-polarized light. **(D)** Mudstone containing abundant marine bioclasts including branchiopod, arthropoda and mollusk, Ling 2 Member, 3,558.63 m, plane-polarized light. **(E)** Silty mudstone, Ling 2 Member, 3,558.68 m, plane-polarized light. **(F)** Bioclastic limestone rich in shallow benthic bioclastics, Ling 2 Member, 3,738.13 m, plane-polarized light. **(G)** Marine shale rich in radiolarian, lower Ling 3 Member, 3,414.91 m, plane-polarized light. **(H)** Marine shale rich in radiolarian, lower Ling 3 Member, 3,414.62 m, and plane-polarized light. **(I)** marine shale rich in detrital quartz, lower Ling 3 Member, 3,412.12 m, plane-polarized light.

RESULTS

Sedimentological Characteristics

Ling 1 Member

Based on observation of typical outcrop and drilling core from the studied well, the lower Ling 1 consist of black shale with interbed of gravity flow sandstone (**Figure 2A**). Scour surface can be observed between gravity flow sandstone and black shale in the core (**Figure 3A**). Above Emeishan basalt belongs to the upper part of Ling 1 Member black shale with multiple interbeds of bentonite (**Figures 2B**, **3B**). Combined with previous study results (Shellnutt et al., 2012), the bentonite interbeds are derived from Emeishan volcanic plume. Under plane-polarized light, thin sections show that black shale with abundant bioclasts including sponge spicule (**Figure 4A**), radiolarian, and mollusk (**Figures 4B,C**) in upper Ling 1 suggest high paleoproductivity.

Ling 2 Member

The Ling 2 member consists of multiple rock types including micritic limestone, mudstone (**Figure 2C**), silty mudstone (**Figure 2D**), siltstone (**Figure 3C**), and bioclastic limestone (**Figure 3D**). Frequent interbeds between different types of sedimentary rock can be observed in core and outcrops (**Figure 3E**). Under plane-polarized light, thin sections show that mudstone in Ling 2 Member is rich in bioclasts including branchiopod, arthropoda, and mollusk (**Figure 4D**). Silty mudstone is rich in silt-sized detrital quartz (**Figure 4E**). Bioclastic limestone in Ling 2 is mainly composed of shallow benthic bioclasts (**Figure 4F**).

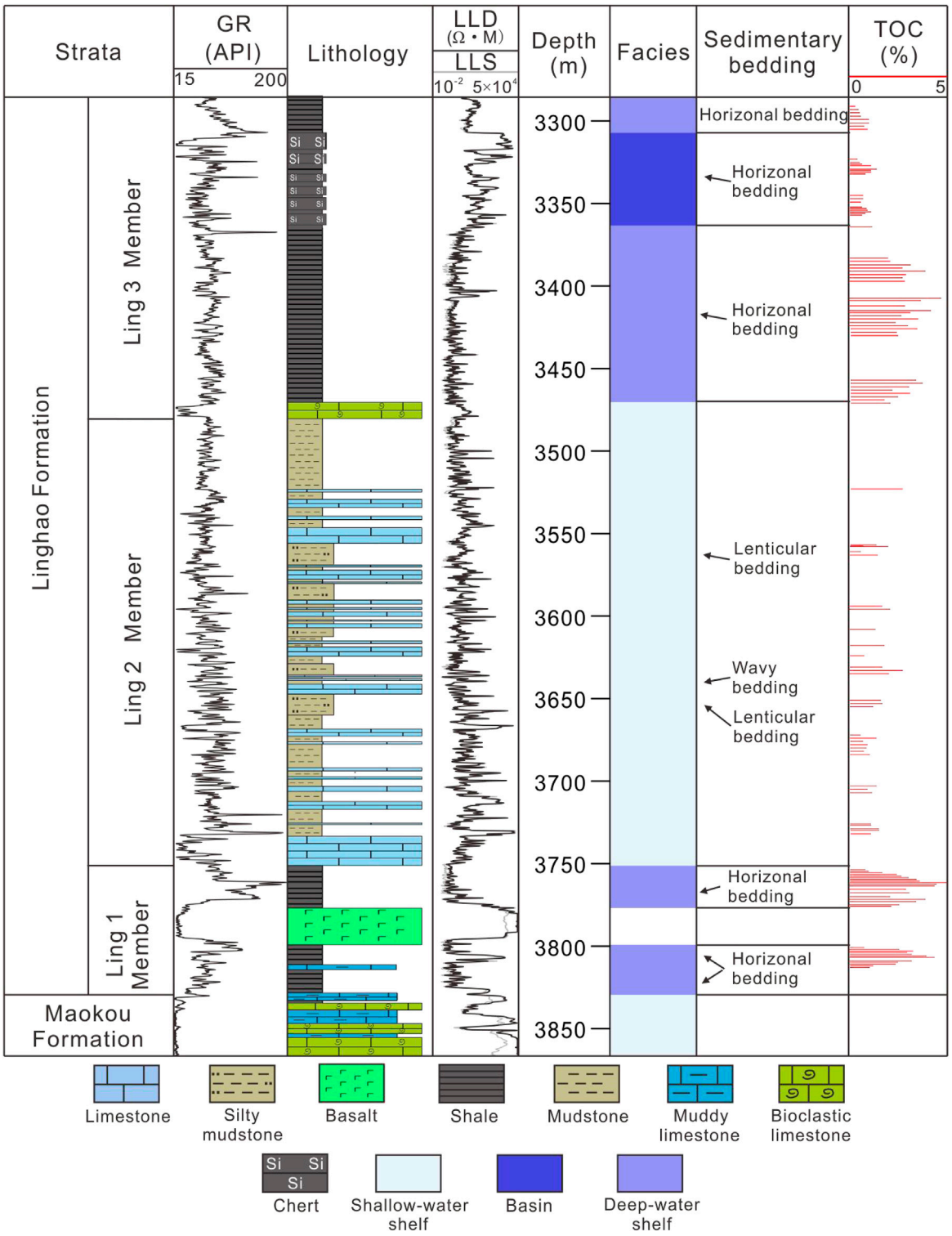

FIGURE 5 | Comprehensive histogram of sedimentary facies of Linghao Formation marine shale from the studied well in the central Nanpanjiang basin.

Ling 3 Member

The lower Ling 3 Member is composed of black shale with horizontal bedding (**Figures 2E,F**). In the core, bentonite interbeds are developed in black shale (**Figures 3F,G**). In certain intervals of black shale in lower Ling 3 (**Figure 3H**), black shale is characterized by massive bedding without any

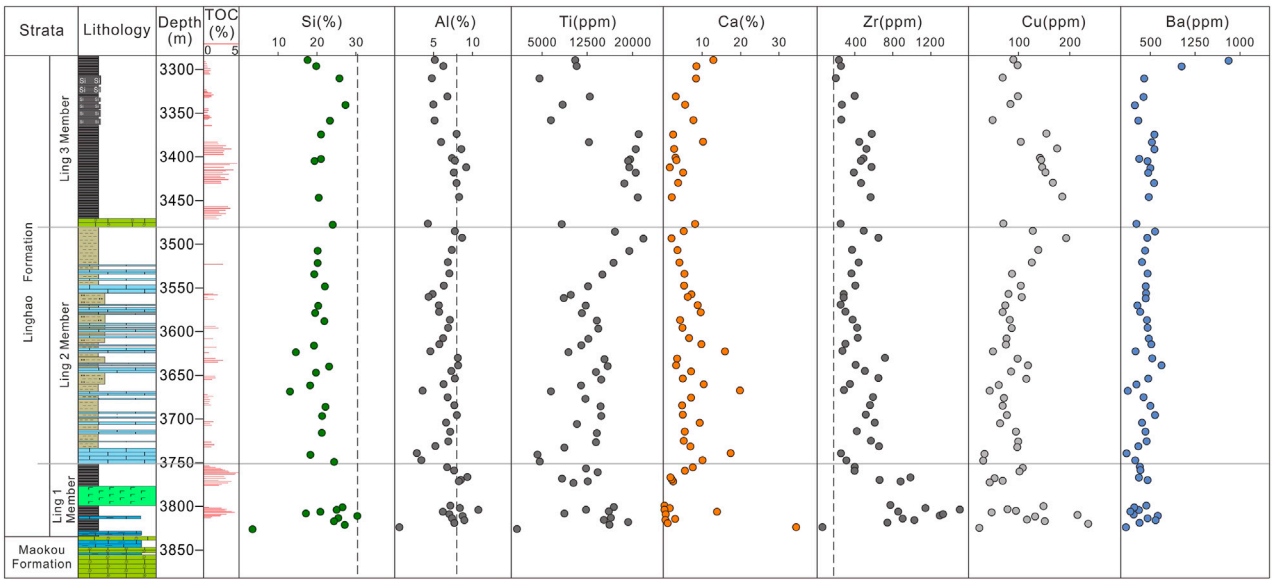

FIGURE 6 | Major and trace elements contents for Linghao Formation marine shale from the studied well in the central Nanpanjiang basin (1). Dashed lines represent the upper continental crust value for the corresponding element (McLennan, 2001)

bioclast (**Figure 4I**). Under plane-polarized light, thin sections show that black shale in lower Ling 3 contains some radiolarian (**Figures 4G–I**). The upper Ling 3 Member is composed of chert layers with horizontal bedding (**Figure 2G**), which is characterized by gravity flow sandstone (**Figure 2H**).

TOC Content Characteristics

Based on the TOC measurement results of marine shale or mudstone (**Figure 5**), the TOC of Ling 1 marine shale varies widely, ranging from 0.14% to 6.36%, with an average of 2.36% (n = 14). The TOC range of marine shale in Ling 2 is relatively small, ranging from 0.50% to 3.08%, and the average value is only 1.30% (n = 19). For lower Ling 3, the range of TOC is 0.58%–4.36%, with an average of 2.43% (n = 9). In upper Ling 3, the range of TOC is 0.79%–3.24%, with an average value of 1.87% (n = 4).

Major Element Content

The major element content of different members in the Linghao Formation is different (**Figure 6**). The Ca content of Ling 2 member is obviously higher, ranging from 2.25% to 19.81%, with an average of 7.40% (n = 31). The content of Ca in Ling 1 is 0.31%–13.90%, with average value of 3.04% (n = 14). The average content of Ca in a high TOC interval (3,756 m–3805 m) is 2.83%. The content of Ca in lower Ling 3 member is 1.17%–10.31%, with an average of 4.26% (n = 10). The Ca content of upper Ling 3 is 3.18%–12.93%, with an average of 8.04% (n = 7).

The Al content and Si content of Ling 1 is relatively higher (**Figure 6**). The average content of Al and Si is 8.08% (6.23%–10.74%, n = 14) and 24.69% (17.26%–30.34%, n = 9), respectively. The average content of Al and Si for Ling 2 is 6.35% (2.96%–8.69%, n = 31) and 20.24% (13.19%-24.48%, n = 19), respectively. The average content of Al and Si for lower Ling 3 is 7.63% (5.21%–9.23%, n = 10) and 21.10% (19.45%–23.38%, n = 5), respectively. The average content of Al and Si in the upper Ling 3 is 5.78% (4.88%–6.96%, n = 7) and 22.07% (17.70%–27.35%, n = 6), respectively. The average content of Ti and Zr in Ling 1 is 13954 ppm (8370–19278 ppm, n = 14) and 924 ppm (399–1508 ppm, n = 14), respectively. The average content of Ti and Zr in Ling 2 is 12260 ppm (4338–21762 ppm, n = 31) and 430 ppm (250–719 ppm, n = 31), respectively. The average content of Ti and Zr in the lower Ling 3 is 17929ppm (6570–21000 ppm, n = 10) and 477 ppm (260–580 ppm, n = 10), respectively. The average content of Ti and Zr in upper Ling 3 is 10136 ppm (4,662–14556 ppm, n = 7) and 284 ppm (200–402 ppm, n = 7), respectively.

Trace Element Content

The content of indicator trace elements or their ratios has been extensively applied to reveal the paleoredox conditions, paleosalinity, paleoclimate, and paleoproductivity of the sedimentary environment. The variation of trace elements and sedimentary environment geochemical indicators of each member are shown in **Figures 7**, **8**. The CIA* of lower Ling 1 is higher than that of the other two members, ranging from 75.94 to 91.90, with an average of only 82.23 (n = 9). The CIA* values of upper Ling 1, Ling 2 and upper Ling 3 are similar, and the average values are 74.33 (73.27-76.32, n = 5), 73.92 (68.96-79.47, n = 31), and 74.08 (72.36-75.03, n = 6), respectively. The CIA* of lower Ling 3 is the highest, ranging from 73.53 to 79.45, with an average of only 77.94 (n = 10).

The variation trend of Sr/Cu is opposite to that of CIA* (**Figure 8**). The Sr/Cu of lower Ling 1 is the lowest, ranging from 0.34 to 20.54, and the average value is only 3.01 (n = 9). The average Sr/Cu ratios for upper Ling 1, Ling 2 and upper Ling 3 is

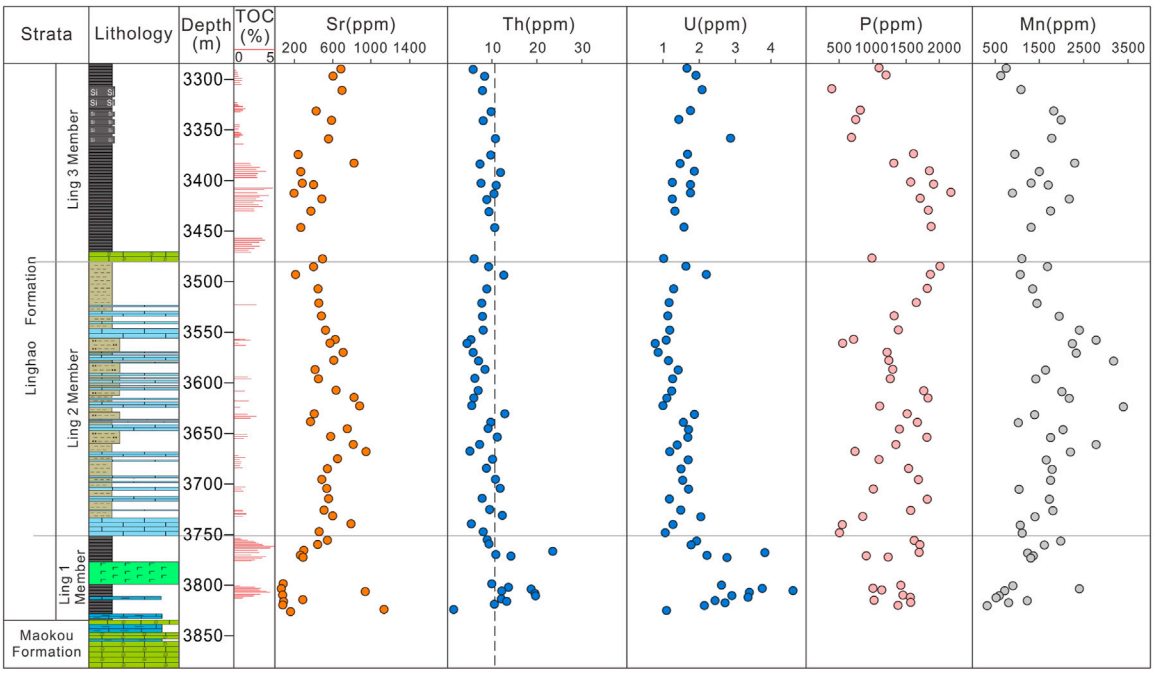

FIGURE 7 | Major and trace elements contents for Linghao Formation marine shale from the studied well in the central Nanpanjiang basin (2). Dashed lines represent the upper continental crust value for the corresponding element (McLennan, 2001)

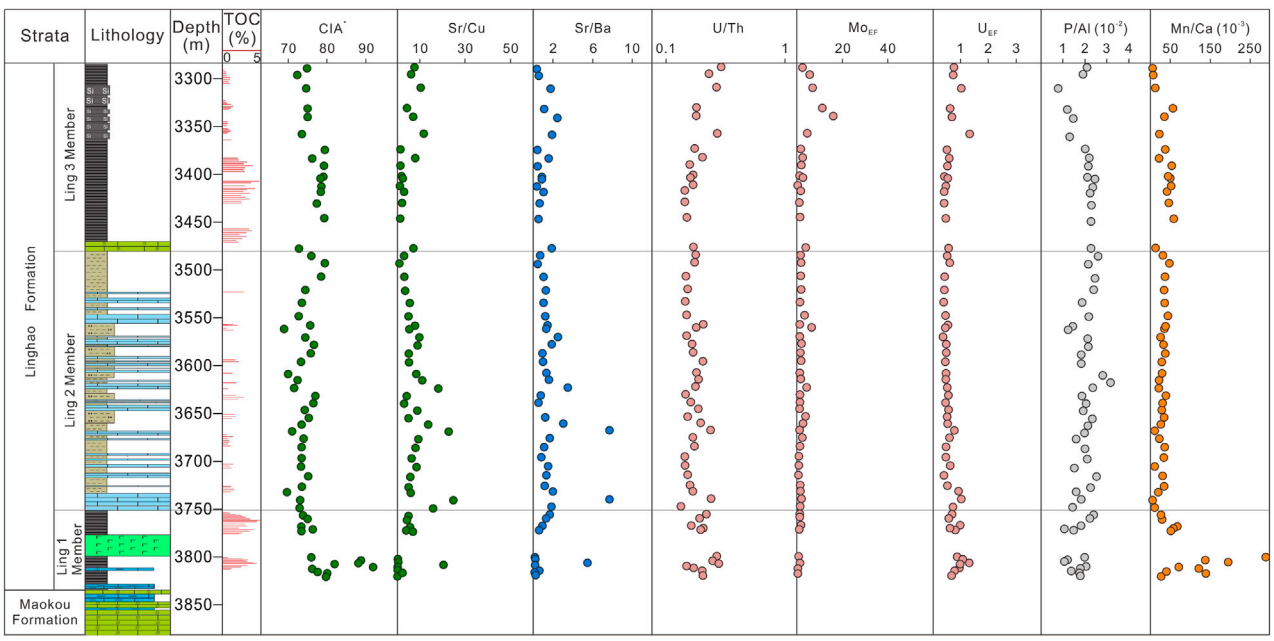

FIGURE 8 | TOC and trace elements ratios for Linghao Formation marine shale from the studied well in the central Nanpanjiang basin.

5.26 (4.02-6.98, n = 5), 8.35 (1.10-24.88, n = 31) and 6.88 (4.39-10.43, n = 6), respectively. The Sr/Cu of lower Ling 3 is relatively low, ranging from 1.36 to 11.77, with an average of only 3.60 (n = 10).

The variation of Sr/Ba is similar to that of Sr/Cu (**Figure 8**). The Sr/Ba of lower Ling 1 is the lowest, ranging from 0.13 to 5.48, and the average value is only 0.85 (n = 9). The average Sr/Ba ratios for upper Ling 1, Ling 2, and upper Ling 3 is 1.04 (0.59-1.69, n =

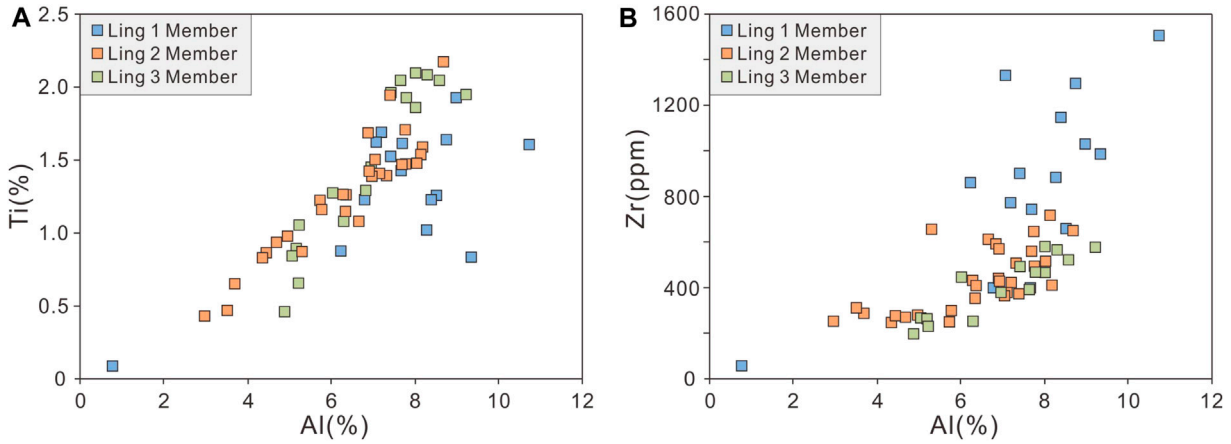

FIGURE 9 | (A) Crossplot of Ti-Al for Linghao Formation marine shale. **(B)** Crossplots of Zr-Al for Linghao Formation marine shale.

5), 1.86 (0.48-7.72, n = 31), and 1.09 (0.22-2.45, n = 6), respectively. The Sr/Ba of lower Ling 3 is relatively low, ranging from 0.40 to 1.90, with an average of only 0.88 (n = 10). The average values of U/Th for each member are similar, and the average value of Ling 1, Ling 2, and Ling 3 is 0.21 (0.15-0.28, n = 14), 0.17 (0.13-0.24, n = 31), and 0.19 (0.14-0.29, n = 16), respectively.

DISCUSSION

Detrital Influx Proxies

As important elements in sedimentary rocks, the contents of Al, Ti, and Zr in rocks are almost not affected by weathering or diagenesis, so these elements are applied for evaluation of the influence degree of terrestrial input (Li et al., 2017; Liu et al., 2021). Al only exists in the clay minerals of fine-grained sedimentary rocks, while Ti and Zr are mainly assigned to clay, sand, and silt particles composed of ilmenite, rutile, and augite (Caplan and Bustin, 1998; Murphy et al., 2000). The detrital influx proxies represented by Al, Ti, and Zr, are generally high for lower Ling 1 (**Figure 6**), especially in the high TOC interval (3,800 m–3807 m). It is suggested that the gravity flow delivered more terrestrial organic matters into the water during the depositional stage of the lower Ling 1. This terrigenous organic matter, on the one hand, provides a lot of nutrients for microbes or directly increases the organic carbon content of shales (Khripounoff et al., 2009). Zr/Al and Ti/Al ratios are thought to closely relate to the coarser part of the sediments (Bertrand et al., 1996; Caplan and Bustin, 1998). Good Ti-Al correlation suggests that Ti comes from the lattice of clay minerals or stable terrigenous clastic materials (Leifu Zhang et al., 2021). Ling 2 and Ling 3 are characterized by good Ti-Al correlation, while Ling 1 is not (**Figure 9A**). It is suggested that the detrital influx of Ling 2 and Ling 3 is relatively stable, while that of Ling 1 is not. Zr usually exists in clay minerals or heavy minerals of silt size (e.g., zircons) (Rachold and Brumsack, 2001; Liu et al., 2017). The correlation between Al and Zr is relatively good for Ling 2 and Ling 3, while Ling 1 is not (**Figure 9B**). The results also show that the detrital influx of Ling 1 is strongly unstable and heterogeneous.

Paleoclimate Conditions

The warm-humid climate is favorable for the atmospheric water cycle, accelerating the chemical weathering intensity, and causing the transportation of nutrients to marine or lakes. Moreover, a warm-humid climate benefits the prosperity of plankton in surface water, and the burial amount of organic matter.

Since the paleoclimate variations will alter the chemical composition of rocks to a certain degree, the paleoclimate of the depositional period can be reflected by the change in the chemical composition of rocks in turn. Sr and Cu are very sensitive to climate change, so the concentrations of these two elements can be applied to illustrate the paleoclimate conditions. Sr is likely to be lost due to weathering or leaching, while Cu is relatively stable (Leifu Zhang et al., 2021). Under the warm conditions, due to strong chemical weathering, Sr is more easily lost, resulting in increased Sr/Cu in sediments. Under dry and hot conditions, the weathering intensity is relatively low, and more Sr elements remain in the parent rock, resulting in lower Sr/Cu values in sediments. For dry and hot climates, Sr/Cu ratio is between 1-5, while for warm and humid climates, Sr/Cu ratio is greater than 5 (Yandoka et al., 2015; Xie et al., 2018). The average Sr/Cu ratio of Ling 1 is only 3.81, especially the Sr/Cu ratio for lower Ling 1 interval is the lowest (**Figure 8**). The average Sr/Cu ratio of Ling 3 is 4.83. The average Sr/Cu ratio of Ling 2 is 8.35, which is significantly higher than that of other members. It is suggested that a relatively dry climate during the depositional stage of Ling 1 and Ling 3 leads to less terrigenous input, which benefits the deposition of organic-rich shale. The relatively high Sr/Cu ratio for Ling 2 indicates that the paleoclimate tends to be warm and humid.

CIA* (Chemical Index of Alteration) has been extensively utilized to reflect the chemical weathering intensity (Nesbitt and Young, 1982; Bai et al., 2015). In general, high CIA* values suggested warm, humid paleoclimate and strong chemical

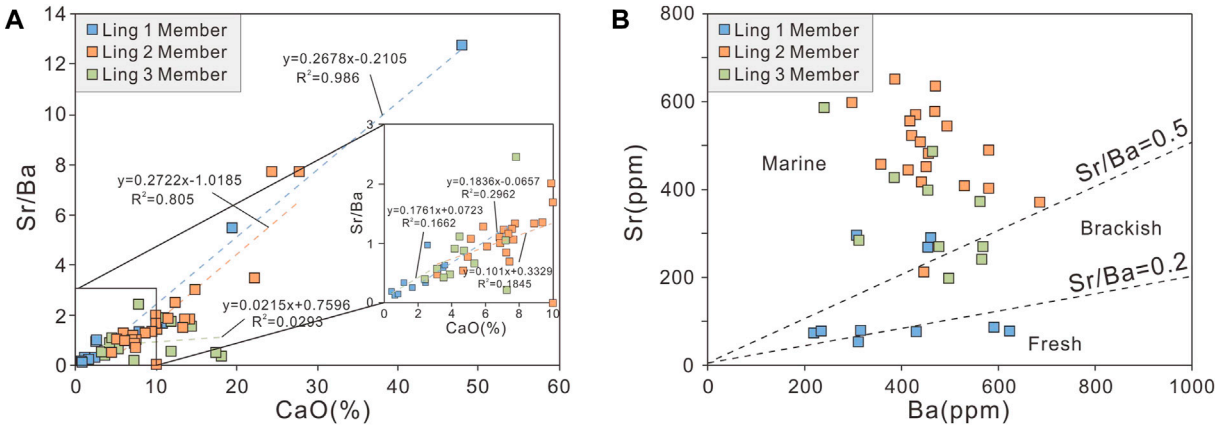

FIGURE 10 | (A) Crossplot between Sr/Ba ratios and CaO concentration of Linghao Formation. **(B)** Paleo-water salinity facies for Linghao Formation.

weathering. Low CIA* values reflect dry and cold paleoclimate, and chemical weathering is weak. Bai et al. (2015) proposed that when CIA* is between 50 and 65, it reflected the cold-dry climate under the background of low chemical weathering. When CIA* is between 65 and 85, it represents the warm-humid climate under the background of moderate chemical weathering. When CIA* is between 85 and 100, it represents the hot and humid paleoclimate under strong chemical weathering. The CIA* for lower Ling 1 is the highest, which is in the middle range (65–85) of chemical weathering. The CIA* values of the Ling 2 and Ling 3 are similar (69–79) (**Figure 8**), which indicates that the climate tends to be warm and humid. It seems that the climate of lower Ling 1 tends to be the warmest and humid interval during the deposition of the Linghao Formation. According to the Sr/Cu ratio and the field outcrop observation results, it is most likely that the high detrital influx represented by gravity flow leads to the high CIA* value in lower Ling 1.

Paleosalinity

Paleosalinity is an important index for restoring the paleosedimentary environment. Ba and Sr were proved to be two indicator elements sensitive to paleosalinity (Wang et al., 1979; Wang, 1996). Sr and Ba showed different enrichment under different salinity. Under low salinity, Ba and Sr existed in soluble bicarbonate. With the increase in salinity, Ba gradually precipitated in the form of $BaSO_4$, and Ba content in water decreased compared to Sr (Wolgemuth and Broecker, 1970). Under higher salinity, Sr is precipitated only in the form of $SrSO_4$ (Wang et al., 1979). The enrichment of Sr in sediments is associated with an increase in salinity, so high Sr/Ba ratios represent an increase in seawater depth and salinity (Chegrouche et al., 2009; Wei and Algeo, 2020). Therefore, Sr/Ba ratio has been extensively applied to qualitatively restore paleosalinity (Wei et al., 2018; Wei and Algeo, 2020). Sr content and Sr/Ba ratio in sedimentary rocks have a strong positive linear relationship with paleosalinity, while Ba content is negatively correlated with paleosalinity. Since Sr and Ca are similar in atomic radius, Sr content may be much higher in sediments containing carbonate components. Before restoring paleosalinity by Sr/Ba ratio, the interference of carbonate rocks on Sr concentration must be excluded.

CaO content was used as a proxy for carbonate content and the positive Sr/Ba–CaO relationships are present in Ling 1 and Ling2 samples with CaO content larger than 10% **(Figure 10A)**. We selected CaO = 10% as the maximum carbonate threshold for Linghao Formation sediments in this study. In **Figure 10B**, the CaO threshold (CaO = 10%) was applied to eliminate samples that probably contained carbonate-hosted Sr Wei and Algeo (2020) proposed that sedimentary Sr/Ba ratios of <0.2, 0.2-0.5, and >0.5 are indicative of freshwater, brackish, and marine water, respectively. Sr/Ba ratios are different in different members **(Figure 8)**. Ling 2 and Ling 3 sediments are deposited in marine environments, and the average Sr/Ba ratio is 1.86 and 0.96, respectively. The Sr/Ba ratio of Ling 1 is higher than that of the other two members, with an average value of 0.40, which represents brackish water-fresh water **(Figure 10B)**. Combined with outcrop observation **(Figure 2A)**, it is suggested that gravity flow may be the direct cause of paleo-water salinity closer to freshwater during the deposition of Ling 1.

Paleoredox Conditions

Trace element proxies including U/Th, U_{EF}, and Mo_{EF} were extensively applied to reveal the redox conditions of paleo-water, and the smaller these proxies represent the higher theoxidation degree, and the larger the ratio represents the stronger the reduction degree (Jian Cao et al., 2018; Liu et al., 2018; Zhang et al., 2019a; He et al., 2020). Previous studies point out that high U/Th ratios were consistent with highly reducing conditions, with U/Th > 1.25 representing dysoxic to anoxic conditions and U/Th < 0.75 representing normal oxic conditions (Hatch and Leventhal, 1992; Jones and Manning, 1994; Tribovillard et al., 2006). Authigenic Mo, authigenic U enrichment, and Mo-U covariant models have been applied to illustrate redox conditions and water mass limitation (Algeo and Lyons, 2006; Algeo and Tribovillard, 2009; Algeo and Liu, 2020). In general, the oxic condition showed little or no enrichment of authigenic U and Mo, while the anoxic conditions showed strong enrichment of authigenic U and Mo (Algeo and Tribovillard,

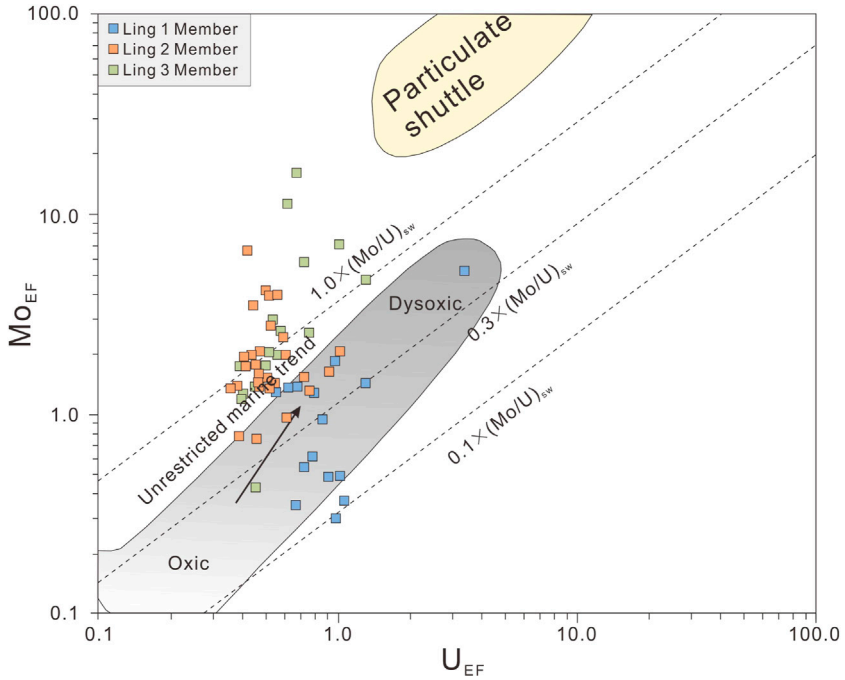

FIGURE 11 | Authigenic Mo-U covariation patterns for Linghao Formation marine shale. The diagonal dashed lines represent the Mo/U molar ratios of the seawater (sw). Grey area represents the "unrestricted marine" trend, characteristic of depositional systems with no limited trace metal renewal. The yellow area represents the "particulate shuttle" trend, characteristic of environments in which intense redox cycling of metals occurs within the water column (Algeo and Tribovillard, 2009; Tribovillard et al., 2012)

2009). The U/Th values of each member are less than 0.75, suggesting that the environment condition of the Linghao Formation is generally inclined to oxic environments (**Figure 8**). The data points of each member are all located between the oxic end and the dysoxic end of unrestricted marine trend (**Figure 11**). It is suggested that the organic-rich shale of Ling 1 and Ling 3 were deposited in an oxic/dysoxic environment. It seems that the redox conditions of Ling 1 and Ling 3 are not favorable for the preservation of organic matter.

Paleoproductivity Proxies

The primary productivity in marine settings is thought to be a significant factor in the formation of organic-rich shales (Liu et al., 2018; Zhang et al., 2019a). As an essential nutrient for plankton, P is widely used to evaluate the primary productivity of the paleomarine environment (Liu et al., 2018; Jian Cao et al., 2018; He et al., 2020). To avoid the influence of the abiotic P from terrigenous input, the P/Al ratio can be used as a proxy for paleoproductivity in a marine environment, using the ratio of Mn/Ca as a reference value (Jian Cao et al., 2018). The P/Al ratio for the lower Ling 1 ranges from 1.06 to 2.06 (average 1.63), and that for upper Ling 1 varies from 1.06 to 2.39 (average 1.80). The P/Al ratio for Ling 2 ranges from 1.23 to 3.17 (average 2.07), and that for lower Ling 3 varies from 1.30 to 2.46 (average 2.14). The P/Al ratio for the upper Ling 3 ranges from 0.78 to 2.44 (average 1.65). It seems that the low P/Al ratio of the Linghao Formation reflects low productivity and the vertical variation trend between TOC and P/Al ratio is not very consistent (**Figure 8**). In contrast, the vertical variation trend between TOC and Mn/Ca ratio is consistent. This phenomenon can be attributed to the effect of redox conditions on enrichment P in sediments (Algeo and Ingall, 2007; Westermann et al., 2013). In reducing environments, P dissolves from sediments into the water, while in oxidizing environments, P is easily adsorbed in Fe compounds (Rimmer et al., 2004), and this could have led to the high TOC and the low ratio of P/Al in the Linghao Formation. Therefore, the low P/Al value in the high TOC intervals of the Linghao Formation does not represent the low paleoproductivity, but on the contrary, represents the high productivity.

SEDIMENTARY MODEL OF ORGANIC-RICH SHALE

Based on the abovementioned discussion, a sedimentary model of organic-rich shale in the Linghao Formation is proposed. The sedimentary environment during deposition of the Maokou Formation is dominated by shallow-water shelves. During lower Ling 1 deposition, the sedimentary environment is dominated by deep-water shelves due to coeval basement-rooted faulting under extension stress background (Changqun Cao et al., 2018; Wang et al., 2022). Strong weathering increases the detrital influx, and active basement-rooted faulting induces frequent gravity flow (**Figure 12A**). Meanwhile, on the one hand, gravity flow brings a large amount of terrestrial organic matter, on the other hand, it provides rich nutrients for plankton and

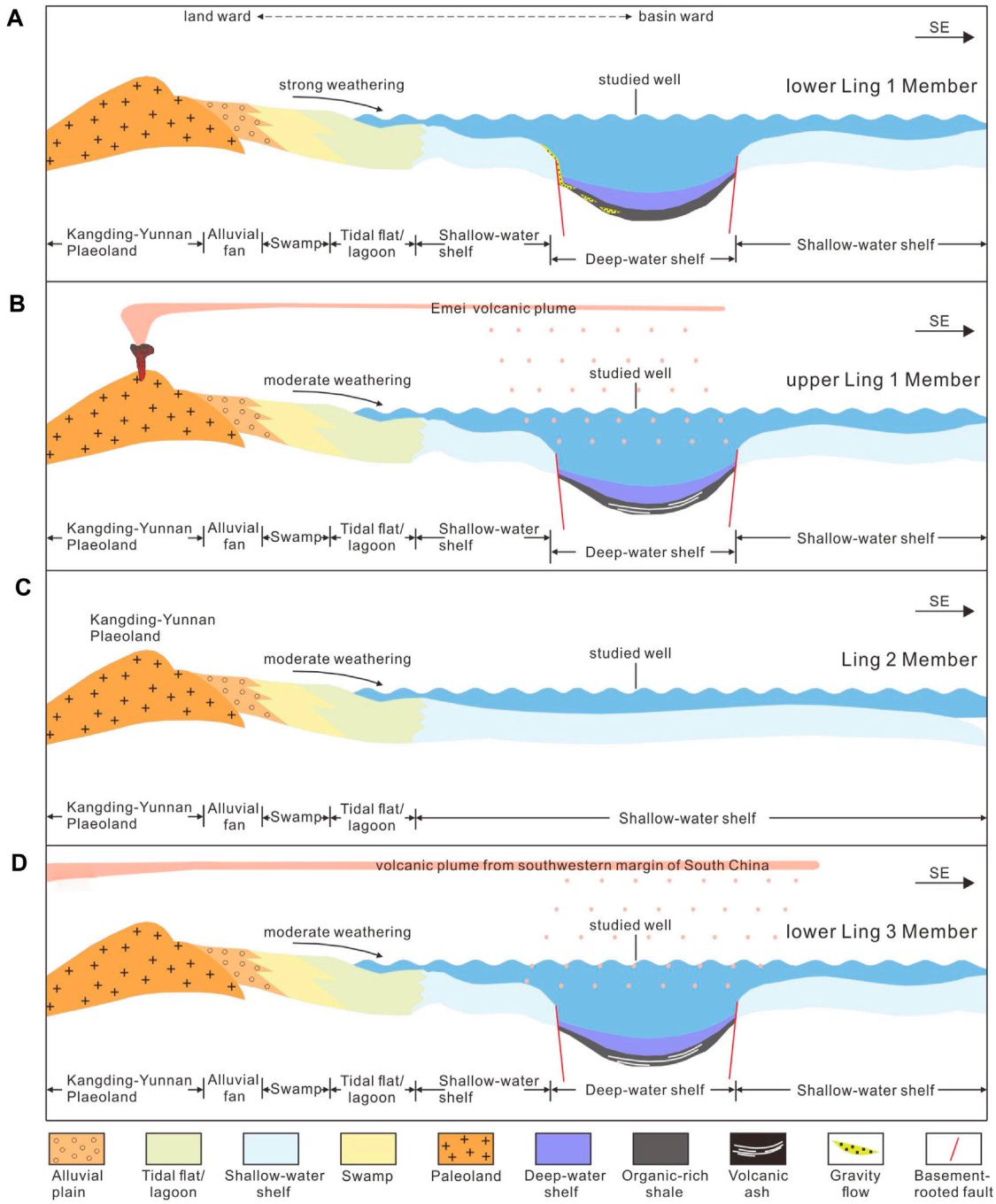

FIGURE 12 | Model of the enrichment mechanisms of organic matters in the Linghao Formation marine organic-rich shale **(A)** lower Ling 1 member. **(B)** Upper Ling 1 member. **(C)** Ling 2 Member. **(D)** Lower Ling 3 member.

improves paleoproductivity (**Figure 12A**). Emeishan volcanic activity formed a set of basalt on lower Ling 1 but did not change the sedimentary environment. The bentonite layers of volcanic ash origin in the organic-rich shale of upper Ling 1 indicate that the volcanic ash benefits the enrichment of organic matter. Firstly, volcanic ash provides biological nutrients for plankton. Secondly, the volcanic ash layer has a strong oxygen insulation ability (**Figure 12B**). During deposition of Ling 2, the sedimentary environment is dominated by shallow-water shelves when basement-rooted faulting entered the dormant period, and this kind of environment is not favorable for organic matter enrichment (**Figure 12C**). With the reactivation of basement-rooted faulting, the sedimentary environment changed into deep-water shelves again during the deposition of lower Ling 3. In

general, the sedimentary model of organic-rich shale in lower Ling 3 is very similar to that in upper Ling 1 (**Figure 12D**), but the difference is that the bentonite in lower Ling 3 originates from felsic volcanism in South China (Wang et al., 2018; Hua Zhang et al., 2021).

CONCLUSIONS

1) There are two organic-rich shale intervals in the Linghao Formation, which are Ling 1 Member and lower Ling 3 Member. Organic-rich shales of these intervals are deposited in the environment of deep-water shelf triggered by basement-rooted faulting under extension stress background.
2) The changes of TOC and its correlation with geochemical proxies suggest that paleoproductivity is the critical factor that controls the enrichment of organic matter during the deposition of Linghao Formation organic-rich shales. For lower Ling 1, detrital influx including gravity flow benefits paleoproductivity, thus controlling the enrichment of organic matter. For upper Ling 1 and lower Ling 3, the volcanic ash of Emei volcanism from Southwest China and felsic volcanism from South China plays a critical role in paleoproductivity, respectively, thus controlling the enrichment of organic matter.

DATA AVAILABILITY STATEMENT

The original contributions presented in the study are included in the article/Supplementary Material; further inquiries can be directed to the corresponding author.

AUTHOR CONTRIBUTIONS

YG contributed as the major author of the article. DH conceived the project. ZW, RL, QX, and JHo collected the samples. ZF, JHn, YW, and YJ analyzed the samples. All authors contributed to the article and approved the submitted version.

FUNDING

This study was funded by the National Science and Technology Major Project of China (Grant number 2017ZX05036) and Science and Technology Cooperation Project of the CNPC-SWPU Innovation Alliance (Grant No. 2020CX030101).

REFERENCES

Algeo, T. J., and Ingall, E. (2007). Sedimentary Corg:P Ratios, Paleocean Ventilation, and Phanerozoic Atmospheric pO2. *Palaeogeogr. Palaeoclimatol. Palaeoecol.* 256 (3–4), 130–155. doi:10.1016/j.palaeo.2007.02.029

Algeo, T. J., and Liu, J. (2020). A Re-assessment of Elemental Proxies for Paleoredox Analysis. *Chem. Geol.* 540, 119549. doi:10.1016/j.chemgeo.2020.119549

Algeo, T. J., and Lyons, T. W. (2006). Mo-total Organic Carbon Covariation in Modern Anoxic Marine Environments: Implications for Analysis of Paleoredox and Paleohydrographic Conditions. *Paleoceanography* 21, a–n. doi:10.1029/2004PA001112

Algeo, T. J., and Tribovillard, N. (2009). Environmental Analysis of Paleoceanographic Systems Based on Molybdenum-Uranium Covariation. *Chem. Geol.* 268, 211–225. doi:10.1016/j.chemgeo.2009.09.001

Bai, Y., Liu, Z., Sun, P., Liu, R., Hu, X., Zhao, H., et al. (2015). Rare Earth and Major Element Geochemistry of Eocene Fine-Grained Sediments in Oil Shale- and Coal-Bearing Layers of the Meihe Basin, Northeast China. *J. Asian Earth Sci.* 97 (97), 89–101. doi:10.1016/j.jseaes.2014.10.008

Bertrand, P., Shimmield, G., Martinez, P., Grousset, F., Jorissen, F., Paterne, M., et al. (1996). The Glacial Ocean Productivity Hypothesis: the Importance of Regional Temporal and Spatial Studies. *Mar. Geol.* 130, 1–9. doi:10.1016/0025-3227(95)00166-2

Caplan, M. L., and Bustin, R. M. (1998). Sedimentology and Sequence Stratigraphy of Devonian-Carboniferous Strata, Southern Alberta. *Bull. Can. Petroleum Geol.* 46 (4), 487–514. doi:10.35767/gscpgbull.46.4.487

Changqun Cao, C., Cui, C., and Zheng, Q. (2018). A Set of Brecciaed-Debris Deposition: Evidence for the Putative Rifting Movement in the Late Guadalupian at Enshi, Hubei Province. *J. Stratigr.* 42 (2), 117–127. doi:10.19839/j.cnki.dcxzz.2018.02.001

Chegrouche, S., Mellah, A., and Barkat, M. (2009). Removal of Strontium from Aqueous Solutions by Adsorption onto Activated Carbon: Kinetic and Thermodynamic Studies. *Desalination* 235 (1-3), 306–318. doi:10.1016/j.desal.2008.01.018

Chen, L., Jiang, Z., Liu, K., Yang, W., Jiang, S., and Tan, J. (2019b). Investigation of Fractal Characteristics and Methane Adsorption Capacity of the Upper Triassic Lacustrine Shale in the SIchuan Basin, Southwest China. *Fractals* 27 (1), 1940011. doi:10.1142/S0218348X19400115

Chen, L., Jiang, Z., Liu, Q., Jiang, S., Liu, K., Tan, J., et al. (2019a). Mechanism of Shale Gas Occurrence: Insights from Comparative Study on Pore Structures of Marine and Lacustrine Shales. *Mar. Petroleum Geol.* 104, 200–216. doi:10.1016/j.marpetgeo.2019.03.027

Chen, L., Liu, K., Jiang, S., Huang, H., Tan, J., and Zuo, L. (2021). Effect of Adsorbed Phase Density on the Correction of Methane Excess Adsorption to Absolute Adsorption in Shale. *Chem. Eng. J.* 420, 127678. doi:10.1016/j.cej.2020.127678

Chen, L., Zuo, L., Jiang, Z., Jiang, S., Liu, K., Tan, J., et al. (2019c). Mechanisms of Shale Gas Adsorption: Evidence from Thermodynamics and Kinetics Study of Methane Adsorption on Shale. *Chem. Eng. J.* 361, 559–570. doi:10.3390/nano903039010.1016/j.cej.2018.11.185

Clarkson, C. R., Jensen, J. L., and Chipperfield, S. (2012). Unconventional Gas Reservoir Evaluation: What Do We Have to Consider? *J. Nat. Gas Sci. Eng.* 8, 9–33. doi:10.1016/j.jngse.2012.01.001

Ding, J., Zhang, J., Tang, X., Huo, Z., Han, S., Lang, Y., et al. (2018). Elemental Geochemical Evidence for Depositional Conditions and Organic Matter Enrichment of Black Rock Series Strata in an Inter-platform Basin: the Lower Carboniferous Datang Formation, Southern Guizhou, Southwest China. *Minerals* 8 (11), 509. doi:10.3390/min8110509

Han, J., Chen, B., Zhao, X., Zheng, C., and Zhang, J. (2017). Development Characteristics and Influential Factors of Organic Pores in the Permian Shale in the Lower Yangtze Region. *Nat. Gas. Ind.* 37 (10), 17–26. doi:10.3787/j.issn.1000-0976.2017.10.003

Hans Wedepohl, K. (1995). The Composition of the Continental Crust. *Geochimica Cosmochimica Acta* 59 (7), 1217–1232. doi:10.1016/0016-7037(95)00038-2

Hatch, J. R., and Leventhal, J. S. (1992). Relationship between Inferred Redox Potential of the Depositional Environment and Geochemistry of the Upper Pennsylvanian (Missourian) Stark Shale Member of the Dennis Limestone, Wabaunsee County, Kansas, U.S.A. *Chem. Geol.* 99 (1/3), 65–82. doi:10.1016/0009-2541(92)90031-y

He, Q., Dong, T., He, S., Zhai, G., Guo, X., Hou, Y., et al. (2020). Sedimentological and Geochemical Characterization of the Upper Permian Transitional Facies of the Longtan Formation, Northern Guizhou Province, Southwest China: Insights into Paleo-Environmental Conditions and Organic Matter Accumulation Mechanisms. *Mar. Petroleum Geol.* 118, 104446. doi:10.1016/j.marpetgeo.2020.104446

Hua Zhang, H., Zhang, F., Chen, J.-b., Erwin, D. H., Syverson, D. D., Ni, P., et al. (2021). Felsic Volcanism as a Factor Driving the End-Permian Mass Extinction. *Sci. Adv.* 7, eabh1390. doi:10.1126/sciadv.abh1390

Huang, B., Yan, Y., Piper, J. D. A., Zhang, D., Yi, Z., Yu, S., et al. (2018). Paleomagnetic Constraints on the Paleogeography of the East Asian Blocks during Late Paleozoic and Early Mesozoic Times. *Earth-Science Rev.* 186, 8–36. doi:10.1016/j.earscirev.2018.02.004

Jia, C. (2017). Breakthrough and Significance of Unconventional Oil and Gas to Classical Petroleum Geology Theory. *Petroleum Explor. Dev.* 44 (1), 1–10. doi:10.1016/S1876-3804(17)30002-2

Jian Cao, J., Yang, R., Yin, W., Hu, G., Bian, L., and Fu, X. (2018). Mechanism of Organic Matter Accumulation in Residual Bay Environments: The Early Cretaceous Qiangtang Basin, Tibet. *Energy fuels.* 32, 1024–1037. doi:10.1021/acs.energyfuels.7b02248

Jones, B., and Manning, D. A. C. (1994). Comparison of Geochemical Indices Used for the Interpretation of Palaeoredox Conditions in Ancient Mudstones. *Chem. Geol.* 111 (111), 111–129. doi:10.1016/0009-2541(94)90085-X

Khripounoff, A., Vangriesheim, A., Crassous, P., and Etoubleau, J. (2009). High Frequency of Sediment Gravity Flow Events in the Var Submarine Canyon (Mediterranean Sea). *Mar. Geol.* 263 (1-4), 1–6. doi:10.1016/j.margeo.2009.03.014

Leifu Zhang, L., Dong, D., Qiu, Z., Wu, C., Zhang, Q., Wang, Y., et al. (2021). Sedimentology and Geochemistry of Carboniferous-Permian Marine-Continental Transitional Shales in the Eastern Ordos Basin, North China. *Palaeogeogr. Palaeoclimatol. Palaeoecol.* 571 (1-3), 110389. doi:10.1016/j.palaeo.2021.110389

Li, Y., Zhang, T., Ellis, G. S., and Shao, D. (2017). Depositional Environment and Organic Matter Accumulation of Upper Ordovician-Lower Silurian Marine Shale in the Upper Yangtze Platform, South China. *Palaeogeogr. Palaeoclimatol. Palaeoecol.* 466, 252–264. doi:10.1016/j.palaeo.2016.11.037

Liang, Q., Tian, J., Zhang, X., Sun, X., and Yang, C. (2020). Elemental Geochemical Characteristics of Lower-Middle Permian Mudstones in Taikang Uplift, Southern North China Basin: Implications for the FOUR-PALEO Conditions. *Geosci. J.* 24, 17–33. doi:10.1007/s12303-019-0008-9

Liang, Q., Zhang, X., Tian, J., Sun, X., and Chang, H. (2018). Geological and Geochemical Characteristics of Marine-Continental Transitional Shale from the Lower Permian Taiyuan Formation, Taikang Uplift, Southern North China Basin. *Mar. Petroleum Geol.* 98, 229–242. doi:10.1016/j.marpetgeo.2018.08.027

Liu, D., Guo, H., Peng, P., and Jia, W. (2013). Characteristics and Controlling Factors of Pore Size Distribution of the Lower Paleozoic Shale Rocks in Lower Yangtze Area. *J. China Coal Soc.* 38 (5), 778–782. doi:10.13225/j.cnki.jccs.2013.05.010

Liu, Q., Li, P., Jin, Z., Liang, X., Zhu, D., Wu, X., et al. (2021). Preservation of Organic Matter in Shale Linked to Bacterial Sulfate Reduction (BSR) and Volcanic Activity under Marine and Lacustrine Depositional Environments. *Mar. Petroleum Geol.* 127, 104950. doi:10.1016/j.marpetgeo.2021.104950

Liu, S., Wu, C., Li, T., and Wang, H. (2018). Multiple Geochemical Proxies Controlling the Organic Matter Accumulation of the Marine-Continental Transitional Shale: A Case Study of the Upper Permian Longtan Formation, Western Guizhou, China. *J. Nat. Gas Sci. Eng.* 56, 152–165. doi:10.1016/j.jngse.2018.06.007

Liu, Z., Algeo, T. J., Guo, X., Fan, J., Du, X., and Lu, Y. (2017). Paleo-environmental Cyclicity in the Early Silurian Yangtze Sea (South China): Tectonic or Glacio-Eustatic Control? *Palaeogeogr. Palaeoclimatol. Palaeoecol.* 466, 59–76. doi:10.1016/j.palaeo.2016.11.007

Luo, W., Hou, M., Liu, X., Huang, S., Chao, H., Zhang, R., et al. (2018). Geological and Geochemical Characteristics of Marine-Continental Transitional Shale from the Upper Permian Longtan Formation, Northwestern Guizhou, China. *Mar. Petroleum Geol.* 89, 58–67. doi:10.1016/j.marpetgeo.2017.06.029

McLennan, S. M. (2001). Relationships between the Trace Element Composition of Sedimentary Rocks and Upper Continental Crust. *Geochem. Geophys. Geosyst.* 2, a–n. doi:10.1029/2000gc000109

Murphy, A. E., Sageman, B. B., Hollander, D. J., Lyons, T. W., and Brett, C. E. (2000). Black Shale Deposition and Faunal Overturn in the Devonian Appalachian Basin: Clastic Starvation, Seasonal Water-Column Mixing, and Efficient Biolimiting Nutrient Recycling. *Paleoceanography* 15, 280–291. doi:10.1029/1999PA000445

Nesbitt, H. W., and Young, G. M. (1982). Early Proterozoic Climates and Plate Motions Inferred from Major Element Chemistry of Lutites. *Nature* 299 (5885), 715–717. doi:10.1038/299715a0

Price, J. R., and Velbel, M. A. (2003). Chemical Weathering Indices Applied to Weathering Profiles Developed on Heterogeneous Felsic Metamorphic Parent Rocks. *Chem. Geol.* 202, 397–416. doi:10.1016/j.chemgeo.2002.11.001

Qiu, Z., and Zou, C. (2020). Controlling Factors on the Formation and Distribution of "Sweet-Spot Areas" of Marine Gas Shales in South China and a Preliminary Discussion on Unconventional Petroleum Sedimentology. *J. Asian Earth Sci.* 194, 103989. doi:10.1016/j.jseaes.2019.103989

Rachold, V., and Brumsack, H. J. (2001). Inorganic Geochemistry of Albian Sediments from the Lower Saxony Basin, NW German: Paleoenvironmental Constraints and Orbital Cycles. *Palaeogeogr. Palaeoclimatol. Palaeoecol.* 174, 123–144. doi:10.1016/s0031-0182(01)00290-5

Rimmer, S. M., Thompson, J. A., Goodnight, S. A., and Robl, T. L. (2004). Multiple Controls on the Preservation of Organic Matter in Devonian-Mississippian Marine Black Shales: Geochemical and Petrographic Evidence. *Palaeogeogr. Palaeoclimatol. Palaeoecol.* 215 (1/2), 125–154. doi:10.1016/s0031-0182(04)00466-3

Sarki Yandoka, B. M., Abdullah, W. H., Abubakar, M. B., Hakimi, M. H., and Adegoke, A. K. (2015). Geochemical Characterisation of Early Cretaceous Lacustrine Sediments of Bima Formation, Yola Sub-basin, Northern Benue Trough, NE Nigeria: Organic Matter Input, Preservation, Paleoenvironment and Palaeoclimatic Conditions. *Mar. Petroleum Geol.* 61, 82–94. doi:10.1016/j.marpetgeo.2014.12.010

Shellnutt, J. G., Denyszyn, S. W., and Mundil, R. (2012). Precise Age Determination of Mafic and Felsic Intrusive Rocks from the Permian Emeishan Large Igneous Province (SW China). *Gondwana Res.* 22 (1), 118–126. doi:10.1016/j.gr.2011.10.009

Tribovillard, N., Algeo, T. J., Baudin, F., and Riboulleau, A. (2012). Analysis of Marine Environmental Conditions Based Onmolybdenum-Uranium Covariation-Applications to Mesozoic Paleoceanography. *Chem. Geol.* 324-325, 46–58. doi:10.1016/j.chemgeo.2011.09.009

Tribovillard, N., Algeo, T. J., Lyons, T., and Riboulleau, A. (2006). Trace Metals as Paleoredox and Paleoproductivity Proxies: An Update. *Chem. Geol.* 232 (1/2), 12–32. doi:10.1016/j.chemgeo.2006.02.012

Wang, A. (1996). Discriminant Effect of Sedimentary Environment by the Sr/Ba Ratio of Different Exising Forms. *Acta Sedimentol. Sin.* 3 (2), 297–304. doi:10.1002/jts.2490030210

Wang, M., Zhong, Y., Hou, Y., Shen, S., Xu, Y., and He, B. (2018). Source and Extent of the Felsic Volcanic Ashes at the Permian-Triassic Boundary in South China. *Acta Petrol. Sin.* 34 (1), 36–48.

Wang, X., Li, B., Yang, X., Wen, L., Xu, L., Xie, S., et al. (2022). Characteristics of "Guangyuan-Wangcang" Trough during Late Middle Permian and its Petroleum Geological Significance in Northern Sichuan Basin, SW China. *Petroleum Explor. Dev.* 48 (3), 655–669. doi:10.1016/S1876-3804(21)60052-6

Wang, Y., Guo, W., and Zhang, G. (1979). Application of Some Geochemical Indicators in Determining of Sedimentary Environment of the Funing Group (Paleogene), Jin-Hu Depression, Kiangsu Province. *J. Tongji Univ.* 2, 51–60.

Wei, W., and Algeo, T. J. (2020). Elemental Proxies for Paleosalinity Analysis of Ancient Shales and Mudrocks. *Geochimica Cosmochimica Acta* 287, 341–366. doi:10.1016/j.gca.2019.06.034

Wei, W., Algeo, T. J., Lu, Y., Lu, Y., Liu, H., Zhang, S., et al. (2018). Identifying Marine Incursions into the Paleogene Bohai Bay Basin Lake System in Northeastern China. *Int. J. Coal Geol.* 200, 1–17. doi:10.1016/j.coal.2018.10.001

Westermann, S., Stein, M., Matera, V., Fiet, N., Fleitmann, D., Adatte, T., et al. (2013). Rapid Changes in the Redox Conditions of the Western Tethys Ocean during the Early Aptian Oceanic Anoxic Event. *Geochimica Cosmochimica Acta* 121, 467–486. doi:10.1016/j.gca.2013.07.023

Wolgemuth, K., and Broecker, W. S. (1970). Barium in Sea Water. *Earth Planet. Sci. Lett.* 8 (5), 372–378. doi:10.1016/0012-821X(70)90110-X

Xi, Z., Tang, S., Wang, J., Yang, G., and Li, L. (2018). Formation and Development of Pore Structure in Marine-Continental Transitional Shale from Northern

China across a Maturation Gradient: Insights from Gas Adsorption and Mercury Intrusion. *Int. J. Coal Geol.* 200, 87–102. doi:10.1016/j.coal.2018.10.005

Xi, Z., Tang, S., Zhang, S., Lash, G. G., and Ye, Y. (2022). Controls of Marine Shale Gas Accumulation in the Eastern Periphery of the Sichuan Basin, South China. *Int. J. Coal Geol.* 251, 103939. doi:10.1016/j.coal.2022.103939

Xi, Z., Tang, S., Zhang, S., and Sun, K. (2017). Pore Structure Characteristics of Marine-Continental Transitional Shale: A Case Study in the Qinshui Basin, China. *Energy fuels.* 31, 7854–7866. doi:10.1021/acs.energyfuels.7b00911

Xia, W., Yan, Q., Xiang, Z., Xia, L., Jiang, W., Wei, W., et al. (2018). Sedimentary Characteristics of the Early-Middle Triassic on the South Flank of the the Xilin Faulted Block in the Nanpanjiang Basin and its Tectonic Implications. *Acta Petrol. Sin.* 34 (7), 2119–2139.

Xie, G., Shen, Y., Liu, S., and Hao, W. (2018). Trace and Rare Earth Element (REE) Characteristics of Mudstones from Eocene Pinghu Formation and Oligocene Huagang Formation in Xihu Sag, East China Sea Basin: Implications for Provenance, Depositional Conditions and Paleoclimate. *Mar. Petroleum Geol.* 92, 20–36. doi:10.1016/j.marpetgeo.2018.02.019

Zhang, K., Jia, C., Song, Y., Jiang, S., Jiang, Z., Wen, M., et al. (2020b). Analysis of Lower Cambrian Shale Gas Composition, Source and Accumulation Pattern in Different Tectonic Backgrounds: A Case Study of Weiyuan Block in the Upper Yangtze Region and Xiuwu Basin in the Lower Yangtze Region. *Fuel* 263 (2020), 115978. doi:10.1016/j.fuel.2019.115978

Zhang, K., Jiang, S., Zhao, R., Wang, P., Jia, C., and Song, Y. (2022). Connectivity of Organic Matter Pores in the Lower Silurian Longmaxi Formation Shale, Sichuan Basin, Southern China: Analyses from Helium Ion Microscope and Focused Ion Beam Scanning Electron Microscope. *Geol. J.* 57, 1912–1924. doi:10.1002/gj.4387

Zhang, K., Peng, J., Liu, W., Li, B., Xia, Q., Cheng, S., et al. (2020c). The Role of Deep Geofluids in the Enrichment of Sedimentary Organic Matter: a Case Study of the Late Ordovician-Early Silurian in the Upper Yangtze Region and Early Cambrian in the Lower Yangtze Region, South China. *Geofluids* 2020, 1–12. doi:10.1155/2020/8868638

Zhang, K., Peng, J., Wang, X., Jiang, Z., Song, Y., Jiang, L., et al. (2020a). Effect of Organic Maturity on Shale Gas Genesis and Pores Development: A Case Study on Marine Shale in the Upper Yangtze Region, South China. *Open Geosci.* 12 (2020), 1617–1629. doi:10.1515/geo-2020-0216

Zhang, K., Song, Y., Jia, C., Jiang, Z., Jiang, S., Huang, Y., et al. (2019b). Vertical Sealing Mechanism of Shale and its Roof and Floor and Effect on Shale Gas Accumulation, a Case Study of Marine Shale in Sichuan Basin, the Upper Yangtze Area. *J. Petroleum Sci. Eng.* 175, 743–754. doi:10.1016/j.petrol.2019.01.009

Zhang, K., Song, Y., Jiang, S., Jiang, Z., Jia, C., Huang, Y., et al. (2019a). Mechanism Analysis of Organic Matter Enrichment in Different Sedimentary Backgrounds: A Case Study of the Lower Cambrian and the Upper Ordovician-Lower Silurian, in Yangtze Region. *Mar. Petroleum Geol.* 99, 488–497. doi:10.1016/j.marpetgeo.2018.10.044

Zou, C., Zhu, R., Chen, Z.-Q., Ogg, J. G., Wu, S., Dong, D., et al. (2019). Organic-matter-rich Shales of China. *Earth-Science Rev.* 189, 51–78. doi:10.1016/10.1016/j.earscirev.2018.12.002

Conflict of Interest: Authors DH, ZW, RL, JHo, ZF, and JHn were employed by Exploration Company of Sinopec.

The remaining authors declare that the research was conducted in the absence of any commercial or financial relationships that could be construed as a potential conflict of interest.

Publisher's Note: All claims expressed in this article are solely those of the authors and do not necessarily represent those of their affiliated organizations, or those of the publisher, the editors, and the reviewers. Any product that may be evaluated in this article, or claim that may be made by its manufacturer, is not guaranteed or endorsed by the publisher.